

## Research Paper

# Nanozyme-mediated catalytic nanotherapy for inflammatory bowel disease

Jiulong Zhao<sup>1,2†</sup>, Wei Gao<sup>3†</sup>, Xiaojun Cai<sup>1,3,✉</sup>, Jijia Xu<sup>2</sup>, Duowu Zou<sup>2,✉</sup>, Zhaoshen Li<sup>2</sup>, Bing Hu<sup>3,✉</sup>, Yuanyi Zheng<sup>1,✉</sup>

1. Shanghai Institute of Ultrasound in Medicine, Shanghai Jiao Tong University Affiliated Sixth People's Hospital, Shanghai 200233 (China)
2. Department of Gastroenterology, Changhai Hospital, Second Military Medical University, Shanghai 200433 (China)
3. Department of Ultrasound in Medicine, Shanghai Jiao Tong University Affiliated Sixth People's Hospital, Shanghai 200233 (China)

†These authors contributed equally to this work.

✉ Corresponding authors: Dr. Xiaojun Cai, c1x2j34@163.com; Prof. Duowu Zou, zdw\_pi@163.com; Prof. Bing Hu, binghu\_stephen@163.com; Prof. Yuanyi Zheng, zhengyuanyi@163.com

© Ivyspring International Publisher. This is an open access article distributed under the terms of the Creative Commons Attribution (CC BY-NC) license (<https://creativecommons.org/licenses/by-nc/4.0/>). See <http://ivyspring.com/terms> for full terms and conditions.

Received: 2019.01.31; Accepted: 2019.02.27; Published: 2019.04.13

## Abstract

The overproduction of reactive oxygen species (ROS) is linked to inflammatory bowel disease (IBD) and causes oxidative damage to DNA, proteins, and lipids. These ROS promote the initiation and progression of ulcerative colitis (UC). This study proposes a unique concept of nanomaterials with intrinsic enzyme-like activity (nanozymes) to mediate catalytic nanotherapy for IBD.

**Methods:** We first synthesized manganese Prussian blue nanozymes (MPBZs) with multi-enzyme activity. A dextran sulfate sodium (DSS)-induced mouse model of colitis was built. The ROS scavenging capacity and anti-inflammatory effects of the MPBZs were investigated.

**Results:** As a proof of concept, MPBZs with multi-enzyme activity were constructed of variable valence elements (Mn and Fe) via a facile and efficient strategy. Due to the increased intestinal permeability and positively charged surfaces of inflamed mucosa in murine colitis, the prepared MPBZs with nanoscale sizes and negative charges preferentially accumulated at inflamed sites after oral administration. Importantly, MPBZs mediated catalytic nanotherapy for IBD in mice via a primary effect on the toll-like receptor signaling pathway without adverse side effects.

**Conclusion:** MPBZs with multi-enzyme activity were constructed to treat IBD. This nanozyme-based approach is a promising strategy for catalytic nanotherapy in patients with colonic IBD.

Key words: nanozyme, multi-enzyme activity, reactive oxygen species, inflammatory bowel disease, manganese Prussian blue

## Introduction

Inflammatory bowel disease (IBD), including ulcerative colitis (UC) and Crohn's disease, is a major problem for many patients worldwide and increases the risk of colorectal cancer [1]. IBD severely decreases quality of life [2]. The pathogenesis of IBD is complicated and poorly understood. There are currently few available therapies that successfully and adequately improve symptoms [3, 4]. Oxidative stress, a key etiological factor of IBD, plays an important role in several of its characteristic signs and symptoms, including abdominal pain, diarrhea, and toxic megacolon [5-7]. During inflammatory episodes,

neutrophils and macrophages infiltrate intestinal mucosa at the sites of IBD and release large amounts of reactive oxygen species (ROS) and cytokines including interleukins (IL)-1 $\beta$ , IL-6, and tumor necrosis factor (TNF)- $\alpha$  [8-12]. Overproduction of ROS causes oxidative damage to DNA, proteins, and lipids, which may promote the initiation and progression of UC [6]. Targeting the sites of inflammation and scavenging ROS may be an efficient strategy to reduce colitis. Most recent studies in animal models have focused on delivery systems to carry antioxidants to diseased intestinal tissues and thereby improve

symptoms of IBD and IBD-associated diseases [13-15]. For example, a nitroxide radical-containing nanoparticle, constructed of a complicated methoxy-poly(ethylene glycol)-b-poly(4-[2,2,6,6-tetramethylpiperidine-1-oxyl] oxymethylstyrene) block copolymer and low-molecular-weight drugs, specifically accumulates in the colonic mucosa to scavenge ROS efficiently for the treatment of colitis via oral administration [16]. Additionally, an H<sub>2</sub>O<sub>2</sub>-responsive  $\beta$ -cyclodextrin nanosystem containing low-molecular-weight drugs was constructed via a nanoprecipitation/self-assembly method and efficiently reduced UC in mice via scavenging ROS and pro-inflammatory cytokines.[17] Nevertheless, the complicated synthesis and multiple components involved in these strategies may impede their clinical translation to IBD therapy [18].

Nanomaterials with intrinsic enzyme-like activities (nanozymes), have shown significant therapeutic potential in various diseases, including Parkinson's disease, cancer, and ischemic stroke [19-22]. Due to their multiple functions, high stability, and easy mass-preparation, nanozymes are a good alternative to traditional enzyme mimetics and natural enzymes in practical applications [21, 23, 24]. Nanozymes also scavenge ROS efficiently via multi-enzyme like activity including superoxide dismutase (SOD), catalase (CAT)-, or peroxidase (POD)-like activities. The most common IBD targeting strategy is size-mediated targeting. Activation of pro-inflammatory cytokines leads to the loss of cellular integrity, subsequently increasing the permeability of intestinal tissue in colitis both at the level of the endothelium and the epithelium [13]. Due to this increased intestinal permeability, nanosystems passively target the inflammatory sites. This may be accompanied by enhanced uptake of nanosystems by infiltrating immune cells [13, 16, 25, 26]. Nanosystems reportedly show size-dependent behavior in IBD: the smaller the particle size, the greater the targeting efficacy and the longer the residence time in inflamed colons [25]. Lamprecht et al. reported that polystyrene particles of 100 nm demonstrated the highest accumulation in inflamed colons among tested particles of 10  $\mu$ m, 1  $\mu$ m, and 100 nm sizes administered orally [26]. In addition, similar size-dependent behavior of polystyrene particles (sizes: 40, 100, 500 nm and 1  $\mu$ m) in a DSS-induced mouse model of colitis were observed by Vong et al. Particles of 40 nm and 100 nm achieved maximal accumulation in inflamed colons [16]. Nanozymes smaller than 100 nm may share this property of size-mediated inflammation targeting to the inflamed colons. Furthermore, the mucus layers of the inflamed colonic mucosa are broken and attract positively

charged proteins [13-15]. Thus, positive charges build up at damaged epithelia. Previous research has demonstrated that nanosystems with negative surface charges target and anchor to inflamed colonic mucosa. For example, Jubeh et al. investigated the differential adhesion of liposomes with different surface charges to healthy and inflamed colons. The results showed that two times more anionic liposomes accumulated at the inflamed colonic mucosa than did cationic or neutral liposomes, while three times more cationic liposomes adhered to healthy colons than did anionic or neutral liposomes [27]. With their intrinsic negative surfaces charges, nanozymes are therefore ideal therapeutic agents for IBD.

Herein, we develop an efficient strategy of nanozyme-mediated catalytic nanotherapy for IBD. Manganese Prussian blue nanozymes (MPBZs) with multi-enzyme activity were constructed via a simple hydrothermal method under facile and mild reaction conditions, which only involved the mixing of the Mn<sup>2+</sup> ion source solution with polyvinylpyrrolidone (PVP) and an [Fe(CN)<sub>6</sub>]<sup>4-</sup> ion source with PVP under magnetic stirring (**Scheme 1A**). Owing to the low redox potential and abundant variable valence states of Mn(II) and Fe(II), MPBZs can act as a new generation of inflammation-targeting ROS nanoscavengers of •OH, H<sub>2</sub>O<sub>2</sub>, and other oxidative factors via multi-enzyme activity. The oral administrated MPBZs prefer to accumulate at the positively charged surfaces of inflamed mucosa in mice with DSS-induced colitis. The MPBZs show a distinct therapeutic efficacy in DSS-induced colitis mice via a primary effect on the toll-like receptor (TLR) signaling pathway without causing any adverse side effects. (**Scheme 1B**). The designed MPBZs will play an important place in the treatment of ROS-associated diseases including acute injuries and chronic diseases.

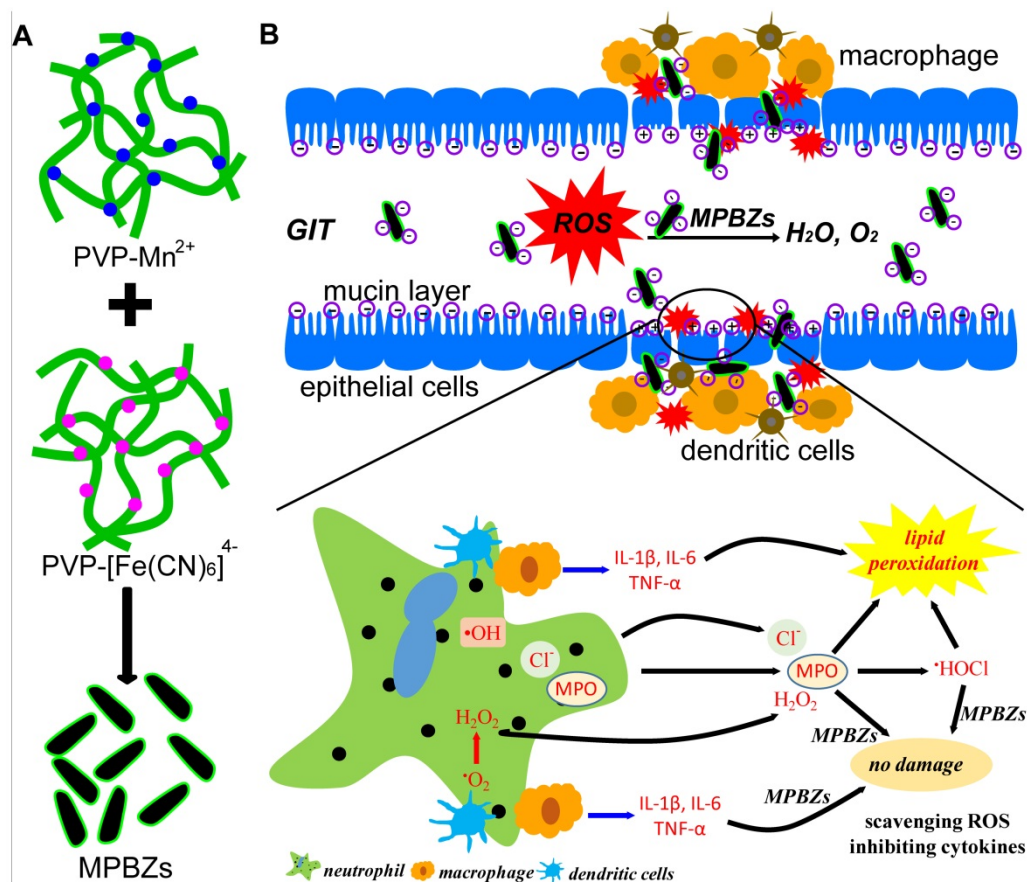
## Methods

### Materials

All chemicals were of analytical grade and used directly without further purification. Manganese chloride (MnCl<sub>2</sub>), potassium ferrocyanide (K<sub>4</sub>[Fe(CN)<sub>6</sub>]), polyvinylpyrrolidone (PVP, K30), fluorescein isothiocyanate (FITC), polyethyleneimine (PEI), and hydrochloric acid were purchased from Adamas-beta, Ltd. (Shanghai, China).

### Synthesis of MPBZs with various sizes and different surface charges

To produce MPBZs of various average hydrodynamic diameters (120, 580, and 870 nm): 0.05 mmol MnCl<sub>2</sub>, 500 mg PVP, and various masses of



**Scheme 1.** (a) Schematic diagram of the synthetic production of MPBZs. MPBZs modified with PVP were constructed via a simple but efficient strategy: mixing the manganese source solution with PVP and an [Fe(CN)<sub>6</sub>]<sup>4-</sup> source with PVP under magnetic stirring. (b) Neutrophils are the principal source of ROS during the inflammatory process. These cells produce •O<sub>2</sub><sup>-</sup> from NOX and NO<sup>+</sup> from inducible nitric oxide synthase (iNOS). H<sub>2</sub>O<sub>2</sub> and Cl<sup>-</sup> are produced by the MPO enzyme, which leads to the production of hypochlorous acid (HOCl). Both MPO and HOCl cause lipid peroxidation and tissue damage. Orally administered MPBZs preferentially adhere to the colonic mucosa through size- and charge-mediated targeting motifs in DSS-induced colitis. Given their excellent size- and charge-mediated targeting motifs, MPBZs have significant therapeutic efficacy in mice with DSS-induced colitis via scavenging ROS and inhibiting proinflammatory cytokines.

trisodium citrate dihydrate (0, 300, and 600 mg) were dispersed into 10 mL distilled water under magnetic stirring for 0.5 h (solution X). Similarly, 0.04 mmol K<sub>4</sub>[Fe(CN)<sub>6</sub>], and 500 mg PVP were dissolved into 10 mL deionized water under magnetic stirring for 0.5 h (solution Y). Solution Y was then added slowly to solution X under magnetic stirring for 1 h, and the final solution was stored without movement (room temperature, 24 h). The precipitate was washed in distilled water several times after centrifugation.

To prepare MPBZs 120 nm in average hydrodynamic diameter with positive surface charges, 0.05 mmol MnCl<sub>2</sub> and 100 mg PEI (MW=10000) were dispersed into 10 mL distilled water under magnetic stirring for 0.5 h (solution E). Similarly, 0.04 mmol K<sub>4</sub>[Fe(CN)<sub>6</sub>] and 100 mg PEI were dispersed into 10 mL distilled water under magnetic stirring for 0.5 h (solution F). Solution F was then added slowly to solution E under magnetic stirring for 1 h. The mixed solution was stored without movement at room temperature for 24 h. The precipitate was washed in distilled water several times after centrifugation.

MPBZs labeled with FITC: 10 mg FITC was added into the MPBZ saline solution (2 mL, 20 mg/mL) with magnetic stirring overnight. MPBZs labeled with FITC were then collected via centrifugation and washed three times with saline solution.

### Measurement of CAT-like activity

We used a specific oxygen electrode on a multi-parameter analyzer (DZS-708; Ningbo Hinotek Technology Co., Zhejiang, China) to investigate generated O<sub>2</sub> in catalase-like activity assays of the MPBZs. In the assay, 1.2 mL 30% H<sub>2</sub>O<sub>2</sub> solution was added to MPBZ PBS solution (pH 7.4, 100 ppm).

### Measurement of SOD-like activity

To measure the SOD-like activity of the MPBZs, a xanthine and xanthine oxidase (XOD) system was chosen. BMPO (5-tert-butoxycarbonyl 5-methyl-1-pyrroline-N-oxide) was selected as the O<sub>2</sub><sup>-</sup> trapping agent. MPBZs at various concentrations (0, 2.5, 5, 10, and 20 mg/L) were added into the xanthine and XOD system before an electron spin resonance test.

### Measurement of the catalytic activities of MPBZs upon elimination of hydroxyl radicals

Electron spin resonance (ESR) with the spin trap reagent BMPO was used to measure hydroxyl radicals ( $\bullet\text{OH}$ ). A typical ESR spectrum with a 1:2:2:1 intensity was obtained. Under UV irradiation (340 nm), commercial  $\text{TiO}_2$  powders generate  $\bullet\text{OH}$ . MPBZs at various concentrations (0, 2.5, 5, 10, and 20 mg/L) were added to 0.1 mg/mL  $\text{TiO}_2$  and 50 mM BMPO in quartz capillary tubes, and then placed in the ESR cavity after UV irradiation or no treatment. ESR spectra were recorded under the following conditions: 20 mW microwave power, 1 G field modulation, 200 G sweep width.

### Cell viability of MPBZs on DLD-1 (epithelial cells of human colorectal adenocarcinoma)

DLD-1 cells with a density of  $2.5 \times 10^4$  cells/well were cultured in 96-well plates for 24 h at  $37^\circ\text{C}$ . Subsequently, MPBZs at various concentrations (0, 20, 40, 80 ppm) were added into the 96-well plates for another 24 h. Cell viability was tested using a Cell Counting Kit-8 proliferation and cytotoxicity assay (Dojindo Molecular Technologies, Inc., Kumamoto, Japan) using a 96-well microplate reader (Victor3).

### The protective effect of MPBZs on LPS (lipopolysaccharide)- $\text{H}_2\text{O}_2$ -activated RAW264.7 macrophages

Raw 264.7 macrophages were initially seeded in triplicate in 6-well plates at a density of  $2.5 \times 10^6$  cells/well for 24 h at  $37^\circ\text{C}$ . Subsequently, the cells were treated with different concentrations of MPBZs (the various concentrations: 0, 2.5, 5, 10 ppm) with or without the stimulation of LPS (10  $\mu\text{g}/\text{mL}$ ) or  $\text{H}_2\text{O}_2$  (400  $\mu\text{M}$ ) for 12 h. The ROS levels were evaluated via flow cytometry.

### Animals

The animal experiments were carried out in accordance with the institutional guidelines of the Animal Care Committee of Shanghai Hospital for IBD Research. Six-week-old male Balb/c mice were purchased from Shanghai Laboratory Animal Center (SLACCAS, Shanghai, China). Mice were specific pathogen-free and fed in cages with temperatures held at  $20\text{--}22^\circ\text{C}$  and relative humidity  $55 \pm 5\%$  on a 12-hour light-dark cycle.

### DSS-induced mouse model of colitis and drug administration

Colitis was induced in the mouse model via the addition of 3% (wt/vol) DSS (MW: 36000–50000; Thermo Fisher Scientific, Waltham, MA, USA) to drinking water for 7 days. The experiment included 3

groups: a normal control group, DSS-injured group, and MPBZ-treated group. The MPBZ solution was orally administered every other day during DSS treatment. On day 9, all mice were sacrificed under isoflurane anesthesia.

### In vivo biodistribution of orally administered MPBZs

MPBZs labeled with FITC (2 mg/kg) saline solution were orally administered to DSS-induced mouse model of colitis. The mice were subjected to abrosia until sacrifice. The mice were sacrificed at various times (2, 6, 12, and 24 h) and their hearts, livers, spleens, kidneys, stomachs, and colons were obtained. Fluorescent images of these organs were obtained using an IVIS small animal fluorescence imaging system (Perkin Elmer). The organs were subsequently dissolved in nitro-muriatic acid for inductively coupled plasma-optical emission spectrometry (ICP-OES) measurement.

### Therapeutic effects of MPBZs on DSS-induced colitis

Mice with DSS-induced colitis and healthy control mice were prepared as described in the previous section. For 9 days, fecal bleeding, changes in body weight, and visible stool consistency were measured. Disease activity index (DAI) is the summation of the stool consistency index (0–3), fecal bleeding index (0–3), and weight loss index (0–4). On the last day of the experiment, mice were sacrificed under ether anesthesia and the entire colon was excised. Distal sections were then prepared for histological assessment. For histological analyses, a 0.5 cm long colon section taken 1 cm from the anus was prepared. The section was first fixed by incubation with 4% (v/v) buffered formalin and 70% (v/v) alcohol, and then embedded in paraffin. Tissue sections of the distal colon were then prepared, stained with hematoxylin and eosin (H&E), and analyzed by microscopy. One hundred milligram of the remaining section was used to measure myeloperoxidase (MPO) activity, malondialdehyde (MDA), ROS,  $\text{H}_2\text{O}_2$ , and the concentrations of IL-1 $\beta$ , IL-6, IFN- $\gamma$  and TNF- $\alpha$ . Using a MPO assay kit (Nanjing Jiancheng Bioengineering Institute, Nanjing, China), Mouse Elisa Kit (Anogen-Yesbiotech, Mississauga, ON, Canada), and a ROS assay kit (Green Fluorescence; Cell Biolabs, Inc, San Diego, CA, USA).

### In vivo biosafety of orally administered MPBZs

Mice were orally administered MPBZs at 18 mg/kg daily for 14 days. The mice were anesthetized and sacrificed to collect the main organs (liver, spleen,

kidney, stomach, and colon) and blood on day 15. The liver, spleen, kidney, stomach, and colons were prepared and stained with H&E. The blood serum was separated from the harvested blood via centrifugation to prepare it for serum biochemistry parameter analyses, including aspartate transaminase (AST) and alanine aminotransferase (ALT) assays. In addition, white blood cells (WBC), hemoglobin (Hb), platelets (PLT), and red blood cells (RBC) were measured using a Sysmex XS-800i automated hematology analyzer (Sysmex Co., Kobe, Japan).

### Real-time polymerase chain reaction (PCR) array and bioinformatics analysis

A PCR array was used to sequence 87 key genes (Table S1) selected from inflammation-related and oxidation-related signaling pathways. The primers used were designed and synthesized by Invitrogen (Carlsbad, CA, USA). The PCR array was designed and produced by BioTNT (Shanghai, China) and used according to the manufacturer's instructions.

### RNA extraction

Thirty milligram tissue sections were weighed and added to 600  $\mu$ L RLT buffer. The tissue was further ground using an electric homogenizer. The supernatant was taken and added to 600  $\mu$ L 70% ethanol after centrifugation. A 700  $\mu$ L sample was placed in an Rneasy spin column. After two centrifugations, 700  $\mu$ L RW1 buffer was added and centrifuged for 1 minute, and the effluent was poured out. Five hundred microliters of RPE buffer was then added to an Rneasy spin column. After two centrifugations, the Rneasy spin column was placed in a prepared 2 mL test tube and centrifuged for 1 minute. Finally, the Rneasy spin column was placed into a prepared 1.5 mL test tube. After centrifugation for 1 minute, 15  $\mu$ L RNase-free water was added and centrifuged for 1 minute to obtain an RNA solution.

### Reverse transcription synthesis of DNA templates

RNA concentrations were normalized for the purpose of this experiment. Using a 100 mL reverse transcription system, reagents were prepared as follows:

**Table 1:** Reverse Transcription System Reagents

	100 $\mu$ L system
RNA Sample	8 $\mu$ L
Oligo (dT) 18	4 $\mu$ L
Reverse Transcription Buffer	20 $\mu$ L
10 mM dNTPmix	5 $\mu$ L
RNase Inhibitor	1.5 $\mu$ L
Reverse Transcriptase	4 $\mu$ L
DEPC Water	56.15 $\mu$ L
Total	100 $\mu$ L

All reagents were added according to the operation steps, and the final cDNA product was stored at -20 °C.

### PCR array

The 384-well plate of the PCR array was stored at -20 °C prior to use (Scheme S1). The premix of RT-PCR dye provided by BioTNT was melted, fully blended, and stored on ice. A 100  $\mu$ L cDNA sample was added with 1 mL PCR water and 1 mL premix to prepare a PCR mixture. The ice layer on the 384 plate was carefully erased and the sealing film was gently torn off. The samples were then added one by one to the 384 plate over ice. Twenty microliters of reaction liquid was accurately added using a new tip for each well.

As shown in the above scheme, a 384-well plate was divided into four regions. We designed 87 target genes and 1 reference gene, so three regions were used and 88 wells were used in each region of the PCR array. A 20  $\mu$ L control mixture was added to the 88 wells in zone 1. Similarly, mixtures from the DSS-induced colitis group and the MPBZ-treated group was added to zones 2 and 3.

RT-PCR was then carried out with a qPCR instrument (ViiA 7, Thermo Fisher Scientific, Waltham, MA, USA).

### PCR array analysis

RT-PCR results were analyzed using the ViiA 7 software. The relative expression level of the target gene was calculated by the  $\Delta\Delta$ Ct method.

### Bioinformatics analysis

Heat maps were drawn using MeV4.9.0. Gene Ontology (GO) and Kyoto Encyclopedia of Genes and Genomes (KEGG) pathway analysis were carried out using STRING.

### Western blotting

#### Sample preparation

A 100 mg sample stored at -80 °C was ground into powder in a mortar filled with liquid nitrogen. Then, 1 mL RIPA lysis buffer was added and centrifuged at 4 °C for 2 minutes. After the supernatant was quantified, all samples were adjusted to the same concentration and the loading buffer was added.

#### Electrophoresis

After gel preparation, protein samples were carefully added one by one, and the marker was added at the same time. Constant voltage electrophoresis (100 V) was used for approximately

100 minutes. When the marker band reached the ideal position, electrophoresis was stopped.

#### Transmembrane transfer

Nitrocellulose (NC) membranes and filter paper were immersed in transfer solution. The glue was retained at 30–100KD, and gel-membrane sandwiches were arranged in the order cassette (black piece)-sponge pad-thick filter paper-NC membrane-gel-thick filter paper-sponge pad-cassette (white piece). A glass rod was used to remove bubbles. The sandwiches were then placed into transmembrane tanks filled with transfer solution at a constant current of 300 mA for 90 minutes at 4 °C.

#### Membrane blocking and antibody incubation

After removal from the tank, the membrane was washed with deionized water and PBST and immersed in the closure solution for approximately 1 h with slow shaking. First, antibodies targeting the proteins NFκB-50, NFκB-105, RELA, TLR4, PTGS1, PTGS2, GAPDH (Proteintech, Rosemont, IL, USA) were added and incubated at room temperature for 1 h and at 4 °C overnight. Afterwards, the membrane was rinsed with TTBS every 10 minutes three times and transferred to horseradish peroxidase solution with slow shaking at room temperature for 1 h. Then, the membrane was rinsed with TTBS every 10 minutes three times.

#### Detection

A and B luminescent solutions of ECL hypersensitive chemiluminescence reagents were diluted in proportion. Each strip was dripped onto 0.2 mL and imaged with an Amersham Imager 600 (GE Healthcare, Chicago, IL USA).

#### Characterization of MPBZs

Transmission electron microscopy (TEM) images were obtained using a JEM-2100F Field Emission Electron Microscope (JEOL, Ltd., Tokyo, Japan) and a field emission Magellan 400 microscope (FEI Company, Hillsboro, OR, USA). Dynamic light scattering (DLS) measurement was carried out on Zetasizer Nano ZS90 (Malvern, Worcestershire, UK).

#### Statistical analysis

All data are presented as means ± SEM unless otherwise indicated. Comparisons between two groups were made using Student's t-test. Escape latencies in the water maze task were compared using repeated measures ANOVA. One-way ANOVA was used for all other multiple-group comparisons. All analyses were carried out using SPSS 19.0. The level of statistical significance was set at  $p < 0.05$ .

## Results and discussion

### Synthesis and characterization of MPBZs

To obtain the desired size and surface charge features, the MPBZs were constructed by reacting  $Mn^{2+}$  with  $[Fe(CN)_6]^{4-}$  under magnetic stirring. MPBZs with good colloidal stability were modified by PVP in the synthetic process without post-modification. The selective  $Mn^{2+}$  and  $[Fe(CN)_6]^{4-}$  ions possess variable valence states, endowing MPBZs with multi-enzyme activity and low redox potential to scavenge ROS efficiently. TEM images revealed discrete and uniform MPBZs of approximately 60 nm in long-axis size (Figure 1A), allowing size-mediated inflammation-targeting of the colonic mucosa [25]. High-resolution TEM images of MPBZs showed a lattice pattern, demonstrating their highly crystalline nature (Figure 1B). Element mapping of MPBZs showed the distributions of K, Fe, and Mn (Figure S1). The X-ray diffraction pattern (Figure 1C) confirmed a manganese Prussian blue analogue composition. The average hydrodynamic diameter of an MPBZ was approximately 120 nm as measured by dynamic light scattering (Figure 1D). We investigated the physiological stability of the MPBZs to ensure their ability to successfully reach sites of inflammation in the colon. The results suggested good stability for at least 3 days in both saline and acidic solutions of pH 1 (Figure S2). The MPBZ solution possessed a negative electric potential of approximately -27.0 mV (Figure 1E), which is vital for the adherence of MPBZs to inflamed colons via the charge-mediated inflammation-targeting strategy [13, 15].

### The effect of MPBZs on ROS

Encouraged by their low redox potential and abundant variable valence states, we subsequently examined whether the MPBZs own the good ROS scavenging property for protecting cells from oxidative damage. There was a significant time-dependent decrease in the hydrogen peroxide concentration after addition of the MPBZs into an aqueous solution of  $H_2O_2$  (Figure 1F). Bubbles could be distinctly seen in the solution after the addition of MPBZs (inset of Figure 1F), which have been confirmed to be oxygen [28]. These results revealed that MPBZs could act as artificial CAT to scavenge  $H_2O_2$ . We then applied the  $TiO_2/UV$  system to investigate the effect of MPBZs on  $\bullet OH$ . The intensity of the characteristic peaks of BMPO/ $\bullet OH$  dramatically decreased as MPBZ concentration increased (Figure 1G, and Figure S3). Thus, the prepared MPBZs have good  $\bullet OH$  scavenging capability [29]. In addition, the constructed MPBZs acting as artificial SOD enzymes efficiently decreased

the intensity of the characteristic peaks of  $\text{BMPO}/\bullet\text{OOH}$  (Figure S4), showing their powerful  $\bullet\text{OOH}$  scavenging ability. We then investigated the effects of MPBZs on the protection of cells suffering from ROS damage. We found that the viability of DLD-1 cells was 90% at an  $80\ \mu\text{g}/\text{mL}$  concentration of MPBZs compared to that in the control group (100%, Figure S5), which indicates that MPBZs have good biocompatibility at the tested concentrations. The protective effects of MPBZs on LPS-/ $\text{H}_2\text{O}_2$ -activated RAW264.7 macrophages were explored. MPBZs greatly alleviated LPS-/ $\text{H}_2\text{O}_2$ -induced oxidative stress by reducing ROS levels (Figure 1H-1I) [30, 31]. This indicated the ROS-scavenging power of the MPBZs, which protected the cells from oxidative stress-induced damage with multi-enzyme activity. The excellent ROS-scavenging properties of the MPBZs can be ascribed to their low electric potential and abundant variable valence states, and suggest their great potential in catalytic nanotherapy for IBD.

### Distribution and biosafety of orally administrated MPBZs

Accumulation of MPBZs at the inflamed mucosa is vital to their therapeutic effects against IBD. DSS-induced colitis mice and normal mice were

treated with MPBZs via oral administration. MPBZs with negative surface charges and nanosizes preferentially accumulated in inflamed colons via size/charge-mediated inflammation targeting (Figure 2A). The UV-vis-NIR spectra of MPBZs before and after mixing with FITC showed the successful construction of FITC-labelled MPBZs (Figure S6). Fluorescence imaging clearly revealed that FITC-labelled MPBZs accumulated at sites of inflammation but not at healthy sites in colons after oral administration (Figure 2B). To reveal the preferential accumulation of MPBZs at inflamed mucosa via a size/charge-mediated inflammation targeting after oral administration, we constructed four kinds of MPBZs of different sizes and surface charges (the average hydrodynamic diameters of MPBZs with negative surface charges: 120 nm, 580 nm, and 870 nm; the average hydrodynamic diameter of MPBZs with positive surface charges: 118 nm; Figure S7). ICP-OES measurement demonstrated that MPBZs 60 nm in size and with negative surface charges showed the highest accumulation at the inflamed mucosa among all the four test groups in the DSS-induced mouse model of colitis (Figure S8). In addition, colons from mice with DSS-induced colitis demonstrated higher MPBZ adherence compared to

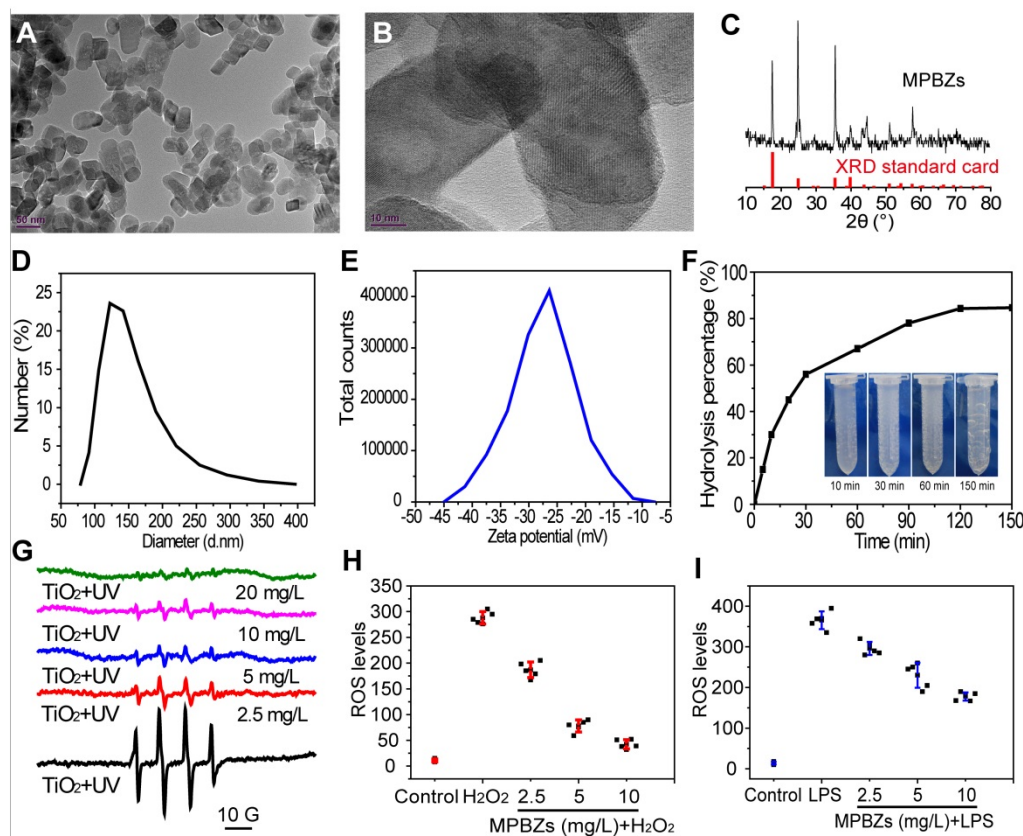


**Figure 1.** (a) TEM images, (b) High-resolution TEM images, (c) XRD pattern, (d) hydrodynamic diameters, and (e) zeta potential of MPBZs. (f) Hydrolysis percentage of  $\text{H}_2\text{O}_2$  after treatment with MPBZs at various time points, as quantified by fluorescence intensity of horseradish peroxidase/dye reagent. (g) The effect of MPBZs on  $\bullet\text{OH}$  levels using the  $\text{TiO}_2$  system. The effects of MPBZs on (h)  $\text{H}_2\text{O}_2$ - and (i) LPS-activated oxidative stress of RAW264.7 macrophages.

control colons (**Figure 2C-D**). These differences can be ascribed to MPBZs accumulating at inflamed mucosa via size/charge-mediated inflammation targeting after oral administration (**Figure 2A**) [13-15, 25, 26, 32]. It is of considerable importance to investigate nonspecific distribution for the in vivo safety of nanomaterials. To precisely investigate the in vivo distribution, we used fluorescence imaging and ICP-OES. The oral administrated MPBZs reached the small intestine and moved to the caecum, and the colon (**Figure 2E-F, and Figure S9**).

The biosafety profile of orally administered MPBZs was further investigated with an administered oral daily dose of 18 mg/kg for 14 days. The mice administrated with saline were the control group. During this 14-day treatment, all the experimented mice appeared normal and showed no unusual behaviors, such as diarrhea, emesis, or tic. There was no difference ( $P < 0.001$ ) between body weights in the control group and MPBZ-treated groups (**Figure S10**). The mice were anesthetized and sacrificed to collect

the main organs (liver, spleen, kidneys, stomach, and colon) and blood after oral administration on day 15. ALT and AST as well as blood urea nitrogen and creatinine remained at normal levels as determined by clinical biochemical analysis, demonstrating no obvious damage to the liver or kidneys induced by MPBZs during the test period (**Figure 3A-B**). In addition, routine blood indices, including WBCs, RBCs, and PLTs, as well as hemoglobin levels in the MPBZ-treated mice were all within the normal ranges, and comparable to those in control mice (**Figure 3C-F**). The H&E staining of liver, spleen, kidneys, stomach, and colon were achieved, and there were no distinguishable abnormalities found in all the H&E staining (**Figure 3G**). Notably, the total uptake of MPBZs into the bloodstream and other organs, including the liver, heart, spleen, and kidneys, was less than 1% (**Figure 2E-F, and Figure S9**). The biosafety experiment showed much lower MPBZ uptake in normal than in diseased tissue, demonstrating a lack of systemic side effects in

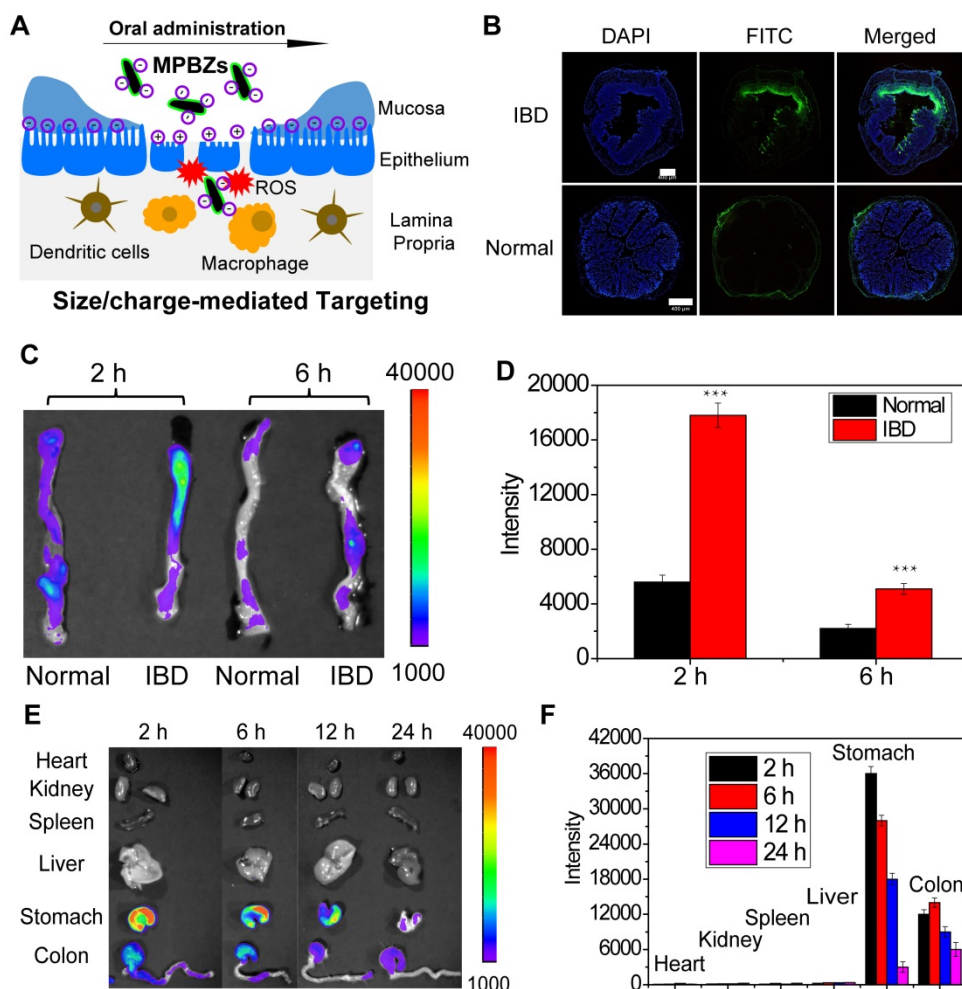


**Figure 2.** (a) After oral administration, MPBZs target the inflamed colon from the epithelium via mechanisms mediated by size and charge. (b) Fluorescence imaging of colons from control mice and mice with DSS-induced colitis after oral FITC-labelled MPBZ treatment. (c) Biodistribution images and (d) corresponding fluorescence intensity values in the colons of mice treated with MPBZs were carried out after oral administration of 2 h and 6 h. Scale bar: 400  $\mu$ m. (e) Biodistribution images and (f) corresponding fluorescence intensity values in the organs of mice treated with MPBZs were measured at various time points after oral administration.

normal tissue (Figure 2E-F). ICP-OES measurements were consistent with those of fluorescence imaging (Figure S9). Although more detailed experimental data should be sought in various animal models, these preliminary results suggest that the orally administrated MPBZs have a good biosafety profile.

### Therapeutic effects of MPBZs on DSS-induced mouse model of colitis

We then evaluated the therapeutic effects of the MPBZs in a DSS-induced colitis mouse model. MPBZs were orally administrated every 2 days to mice with DSS-induced colitis for 7 days. The therapeutic efficacy of MPBZs was evaluated on day 9 (Figure 4A). Body weight was significantly lower in mice with DSS-induced colitis than in control mice. Conversely, mice with colitis in the MPBZ-treated group exhibited a steady weight (Figure S11). DAI is the summation of the stool consistency index, fecal bleeding index, and weight loss index. DAI in mice with DSS-induced colitis showed significant reduce with treatment of oral administrated MPBZs (Figure S12). Colon length is vital in the assessment of therapeutic efficacy in colitis. Compared to the colons of the normal mice ( $7.47\pm 1.04$  cm), the colons in the mice with colitis were significantly shorter ( $4.37\pm 0.58$  cm), and showed signs

of bleeding, indicating successful establishment of the DSS-induced colitis mouse model (Figure 4B and Figure S13). In contrast, mice with colitis that were orally administrated MPBZs exhibited less colon shortening ( $5.97\pm 0.68$  cm), and much less bleeding, and less abnormal stools than those of mice with colitis (Figure 4B and Figure S13). Additionally, stool consistency and fecal bleeding of mice were improved in the MPBZ-treated group. The number of white and red blood cells, as well as hemoglobin level, in the mice with colitis were abnormal relative to those in control mice, which can be mainly ascribed to neutrophil invasion and hemorrhage. However, these parameters in MPBZ-treated mice with colitis returned to normal levels, and were not significantly different from those in control mice (Figure S14). We then further examined histological sections. H&E-stained colons of mice suffering from colitis showed serious necrocytosis, damaged mucous membranes, increased inflammatory cell infiltration, and destroyed crypt structures (Figure 4C). However, a nearly normal histological microstructure was observed in MPBZ-treated mice with colitis, and was even comparable to that observed in control mice (Figure 4C).

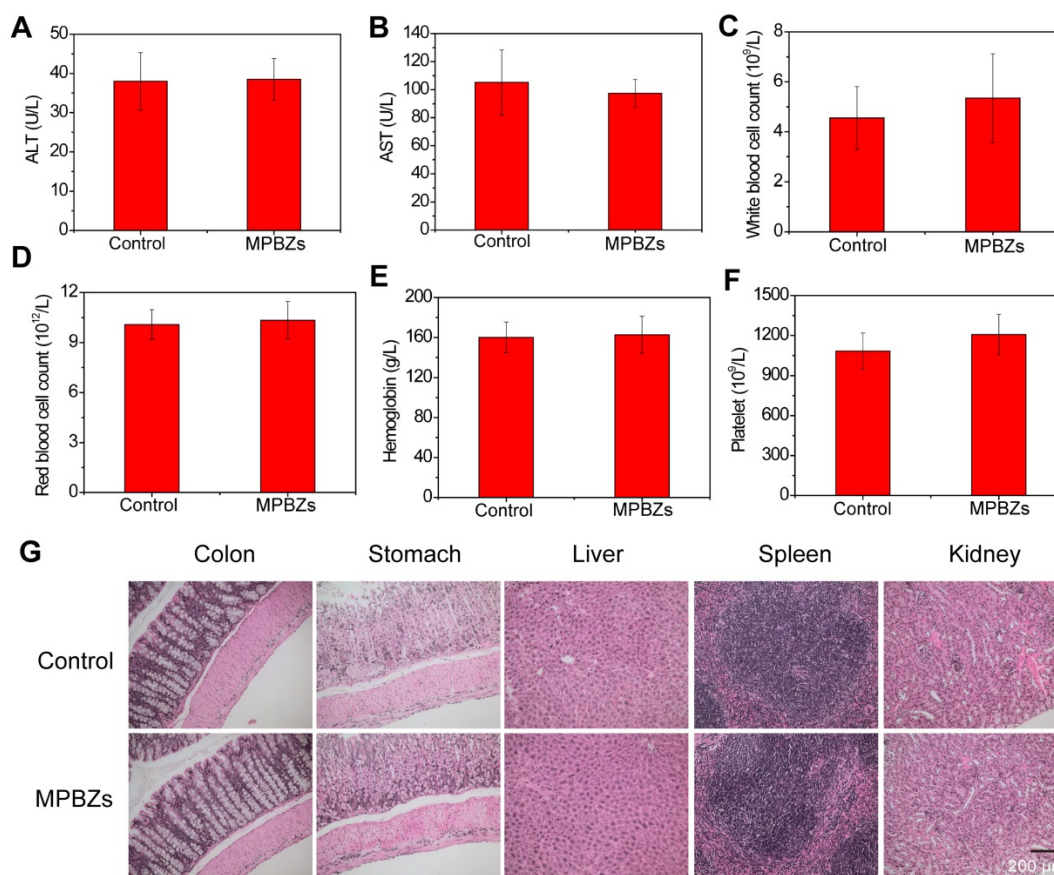


**Figure 3.** (a) The ALT and (b) AST levels of mice in the control and MPBZ-treated groups. Hematological analyses, including (c) white blood cells, (d) red blood cells, (e) hemoglobin, and (f) platelet levels, in mice from the control and MPBZ-treated groups. (g) H&E staining of the colon, stomach, liver, spleen, and kidneys of mice in the control and MPBZ-treated groups. Scale bar: 200  $\mu$ m.

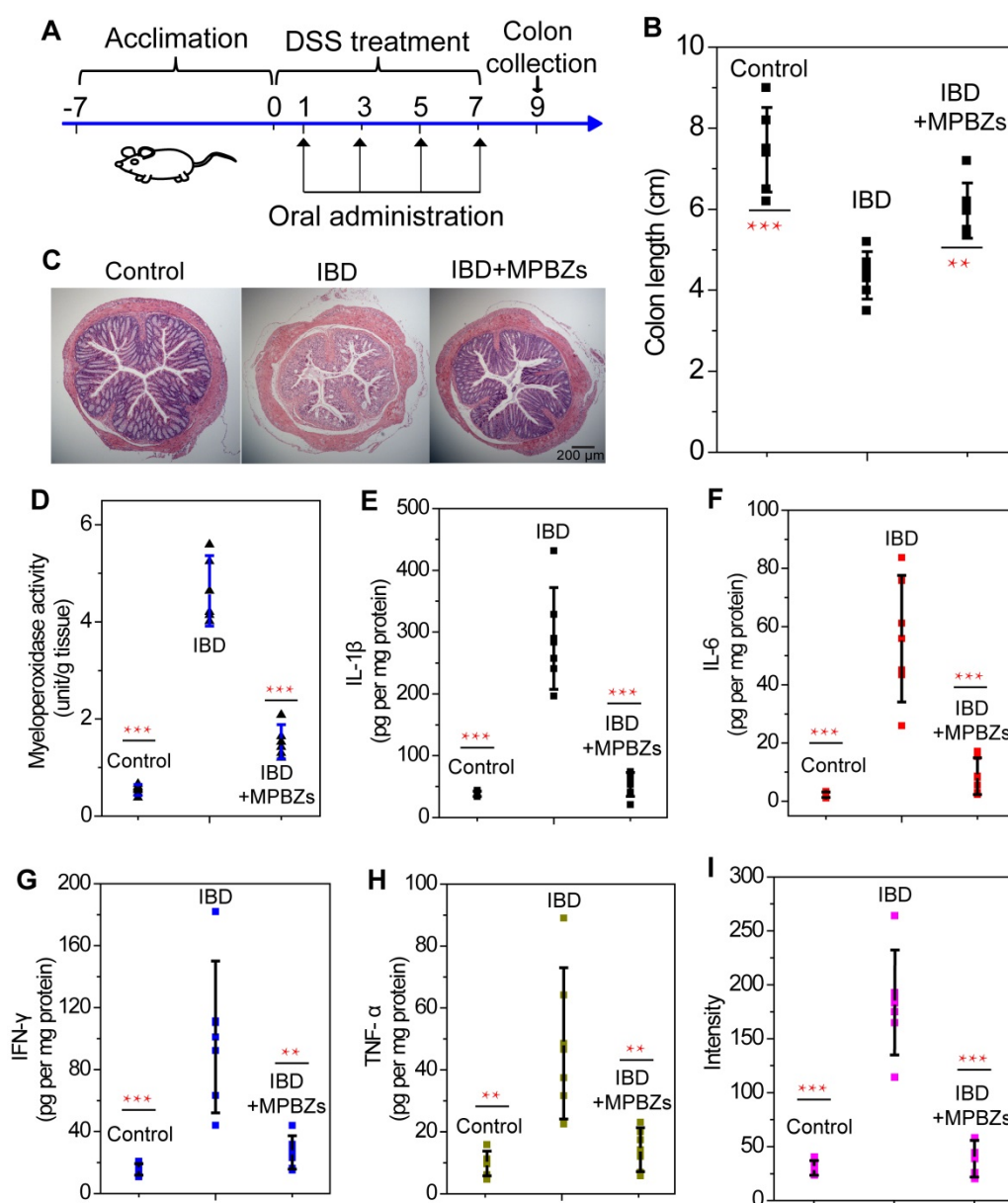


**Figure 4.** (a) Overall experimental procedure. Mice were provided normal water or water containing 3% DSS for 7 days. MPBZs (0.3 mg/mL, 0.3 mL) were orally administered every 2 days to mice with DSS-induced colitis for 7 days, and therapeutic efficacy was assessed on day 9. (b) Length of colonic tissues isolated from mice after 7 days of treatment. (c) H&E-stained histological sections of colonic tissues from mice subjected to various treatments. Scale bar: 200  $\mu$ m. (d) Levels of MPO activity. Changes in proinflammatory cytokine levels in mice from various groups. Levels of (e) IL-1 $\beta$ , (f) IL-6, (g) IFN- $\gamma$ , and (h) TNF- $\alpha$ . After 7 days of treatment, homogenates of the colonic tissues were prepared on day 9, and the concentrations of various mediators were separately measured by commercial kits. The total protein level was measured by the BCA assay. (i) ROS levels in various groups. After 7 days of treatment, homogenates of the colonic tissues were prepared on day 9.

To examine possible mechanisms responsible for the therapeutic and suppressive effects of MPBZs on IBD, different proinflammatory mediators in colonic tissues were tested in detail. MPO demonstrates the extent of neutrophil infiltration in the inflamed colon and is closely correlated with IBD severity. MPO was highly elevated in inflamed colons ( $4.17 \pm 1.21$  unit/g tissue) compared to that in normal colons ( $0.55 \pm 0.14$  unit/g tissue) and was markedly reduced in the MPBZ-treated group ( $1.73 \pm 0.53$  unit/g tissue, **Figure 4D**). The concentration of MDA can reveal the degree of membrane lipid peroxidation, and even the damage of the membrane system. The MDA

concentration in mice with colitis was  $1.86 \pm 0.37$  nmol/mL, higher than that in control mice ( $0.98 \pm 0.30$  nmol/mL), demonstrating the severe damage caused by membrane lipid peroxidation (**Figure S15**). After treatment with MPBZs, the MDA concentration decreased to  $1.18 \pm 0.14$  nmol/mL (**Figure S15**), which was not significantly different ( $P=0.539$ ) from that in control mice. Another indication of colitis severity is proinflammatory cytokine levels. Notably, the IL-1 $\beta$ , IL-6, IFN- $\gamma$  and TNF- $\alpha$  levels in the colonic tissue were significantly lower in MPBZ-treated mice with colitis than those in mice with DSS-induced colitis without MPBZ treatment (**Figure 4E-H**). Importantly,

there were no significant differences between IL-1 $\beta$  (P=0.849), IL-6 (P=0.682), IFN- $\gamma$  (P=0.795), or TNF- $\alpha$  (P=0.862) levels in the IBD+MPBZs and the control groups (**Figure 4E-H**). Additionally, much higher levels of ROS and H<sub>2</sub>O<sub>2</sub> were detected in the inflamed colons than in those of control mice. MPBZ treatment reduced the expression of ROS and H<sub>2</sub>O<sub>2</sub>, which was not significantly different from those observed in the normal mice (**Figure 4I and Figure S16**). Therefore, the prepared MPBZs efficiently alleviated oxidative stress and inhibited proinflammatory cytokines in the colons of mice suffering from colitis. These data clearly demonstrated that the prepared MPBZs with multi-enzyme activity acted as an effective therapeutic agent in IBD, and therefore played a big part in the treatment of inflammation-associated diseases.

### Probable mechanism of MPBZ-mediated nanotherapy for IBD

Further, we explored the probable mechanism of MPBZ-mediated nanotherapy for IBD. Firstly, the high throughput cDNA sequencing method RNA-Seq was selected to fully evaluate the anti-inflammatory effect of MPBZs in the DSS-induced colitis mouse model. A total of 89 genes associated with oxidation and inflammation were selected. Of these 89 DSS-responsive genes, 84 were upregulated and 5 exhibited no significant change compared to those in the control group (**Figure S17**). MPBZ administration suppressed expression of 78 genes upregulated by DSS stimulation. Overall, approximately 93% of genes upregulated by DSS in mice were suppressed by MPBZs, demonstrating the excellent therapeutic potential of MPBZs in combating oxidative and inflammatory stress by modulating associated genes. The top 53 differentially expressed genes, including 34 inflammation-associated (**Figure 5A**) and 19 oxidation-associated genes (**Figure 5B**) were selected to carry out pathway and gene ontology (GO) analysis for the better classification of the biological processes modulating via MPBZs in the DSS-induced mouse model of colitis. Several key inflammatory pathways strongly related with the pathogenesis of a large number of inflammatory diseases, including the TLR signaling pathway, TNF signaling pathway, IBD, and NF $\kappa$ B signaling pathway were inhibited with MPBZ treatment (**Figure S18**), demonstrating the extensive immunomodulatory activity of MPBZs. MPBZs may reduce colitis in mice via a primary effect on the TLR signaling pathway. Target proteins of MPBZs in mice with colitis include TLR4, RELA, NF $\kappa$ B1, TLR2, IL-6, and TNF, among others, and could represent potential therapeutic targets for IBD and other inflammatory diseases. We then validated the effects of MPBZs on

the key proteins in the TLR signaling pathway, including NF $\kappa$ B1, RELA, and TLR4, via western blotting. The expression levels of NF $\kappa$ B1 (NF $\kappa$ B-50 and NF $\kappa$ B-105), RELA, and TLR4 increased in mice with colitis compared to levels in control mice (**Figure 5C**). MPBZ treatment drastically decreased these levels. GO analysis of 19 oxidation-associated genes indicated that MPBZs may mainly inhibit the biological process of response to oxidative stress, which plays an alternative role in ROS regulation to achieve therapeutic effects against IBD (**Figure S19**). The oxidative stress-associated key proteins, including PTGS1 and PTGS2, were investigated via western blotting. In mice with colitis, levels of PTGS1 and PTGS2, which participate in a variety of ROS metabolic reactions, were considerably higher than those in control mice (**Figure 5C**). However, MPBZ treatment regulated PTGS1 and PTGS2 expression, indicating the therapeutic effect of MPBZs on colitis (**Figure 5C**). Therefore, the constructed MPBZs mediated catalytic nanotherapy for IBD in mice via a primary effect on the TLR signaling pathway without adverse side effects.

### Conclusions

In summary, biocompatible MPBZs with multi-enzyme activity were successfully constructed and mediated catalytic nanotherapy for IBD. Owing to their low redox potential and abundant variable valence states, the constructed MPBZs represent a new generation of inflammation-targeting ROS nanoscavengers of  $\bullet$ OH, H<sub>2</sub>O<sub>2</sub>, and other oxidative factors via multi-enzyme activity. The designed MPBZs preferentially accumulate at inflamed mucosa with positively charged artificial surfaces in DSS-induced colitis mice via size/charge-mediated inflammation-targeting strategies. The MPBZs significantly improved colitis in mice via a primary effect on the TLR signaling pathway without causing adverse side effects. These cheap, highly stable MPBZs with multi-enzyme activity represent a promising therapeutic agent for the treatment of IBD and may be a harbinger for the use of active manganese Prussian blue nanozyme-based therapies for ROS-associated diseases, including acute injuries and chronic diseases.

### Abbreviations

ROS: reactive oxygen species; IBD: inflammatory bowel disease; UC: ulcerative colitis; MPBZ: manganese Prussian blue nanozymes; DSS: dextran sulfate sodium; TLR: toll-like receptor; IL: interleukins; TNF: tumor necrosis factor; PVP: polyvinylpyrrolidone; PEI: polyethyleneimine; FITC: fluorescein isothiocyanate; CAT: catalase; POD:

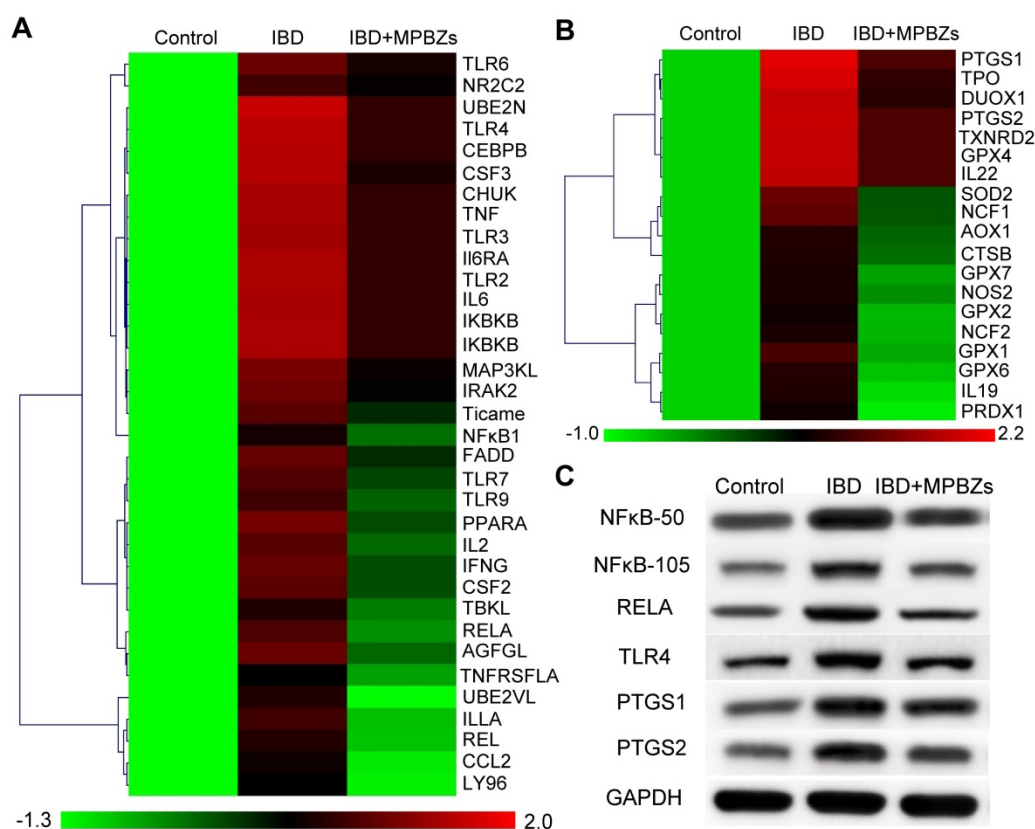


**Figure 5.** (a) Heat map of cytokine profiles from a multiplexed cytokine assay of mice in various groups. (b) Heat map of cytokines associated with antioxidant profiles from a multiplexed cytokine assay of mice in various groups. (c) Expression levels of NFκB-50, NFκB-105, RELA, TLR4, PTGS1, and PTGS2 in various groups.

peroxidase; SOD: superoxide dismutase; TMB: 3,5,3',5'-tetramethylbenzidine; XOD: xanthine oxidase; ESR: electron spin resonance; BMPO: 5-tert-butoxycarbonyl 5-methyl-1-pyrroline-N-oxide; LPS: lipopolysaccharide; ICP-OES: inductively coupled plasma-optical emission spectrometry; DAI: disease activity index; H&E: hematoxylin and eosin; MPO: myeloperoxidase; MDA: Malondialdehyde; WBC: white blood cell; Hb: haemoglobin; PLT: platelet; RBC: red blood cells; PCR: Polymerase Chain Reaction; TEM: transmission electron microscope; DLS: Dynamic light scattering; iNOS: inducible-nitric oxide synthase; HOCl: hypochlorous acid; AST: aspartate transaminase; ALT: alanine aminotransferase; GO: gene ontology.

## Supplementary Material

Supplementary figures, table and scheme.  
<http://www.thno.org/v09p2843s1.pdf>

## Acknowledgements

This research is financially supported by the National Natural Science for Distinguished Young Scholars (Grant No. 81425014), National Natural Science Foundation of China (Grant No. 81370493, No. 81670485), Shanghai Collaborative Innovation Center for Translational Medicine (TM201724), Shanghai key

discipline of medical imaging (NO. 2017ZZ02005), and Shanghai Sailing Program (No. 18YF1419000).

## Competing Interests

The authors have declared that no competing interest exists.

## References

- Podolsky DK. Inflammatory bowel disease. *N Engl J Med.* 2002; 347: 417-29.
- Hoivik ML, Moum B, Solberg IC, Cvancarova M, Hoie O, Vatn MH, et al. Health-related quality of life in patients with ulcerative colitis after a 10-year disease course: results from the IBSEN study. *Inflamm Bowel Dis.* 2012; 18: 1540-9.
- Takedatsu H, Mitsuyama K, Torimura T. Nanomedicine and drug delivery strategies for treatment of inflammatory bowel disease. *World J Gastroenterol.* 2015; 21: 11343-52.
- Khor B, Gardet A, Xavier RJ. Genetics and pathogenesis of inflammatory bowel disease. *Nature.* 2011; 474: 307-17.
- Dagli U, Balk M, Yucel D, Ulker A, Over H, Saydam G, et al. The role of reactive oxygen metabolites in ulcerative colitis. *Inflamm Bowel Dis.* 1997; 3: 260-4.
- Zhu H, Li YR. Oxidative Stress and Redox Signaling Mechanisms of Inflammatory Bowel Disease: Updated Experimental and Clinical Evidence. *Exp Biol Med.* 2012; 237: 474-80.
- Bhattacharyya A, Chattopadhyay R, Mitra S, Crowe SE. Oxidative Stress: An Essential Factor in the Pathogenesis of Gastrointestinal Mucosal Diseases. *Physiol Rev.* 2014; 94: 329-54.
- Piechota-Polanczyk A, Fichna J. Review article: the role of oxidative stress in pathogenesis and treatment of inflammatory bowel diseases. *N-S Arch Pharmacol.* 2014; 387: 605-20.
- Jena G, Trivedi PP, Sandala B. Oxidative stress in ulcerative colitis: an old concept but a new concern. *Free Radical Res.* 2012; 46: 1339-45.
- Thomson A, Hemphill D, Jeejeebhoy KN. Oxidative stress and antioxidants in intestinal disease. *Dig Dis (Basel, Switzerland).* 1998; 16: 152-8.
- Roesser A, Kuester D, Malfertheiner P, Schneider-Stock R. Oxidative stress in ulcerative colitis-associated carcinogenesis. *Pathol Res Pract.* 2008; 204: 511-24.

12. Kawanishi S, Hiraku Y, Pinlaor S, Ma N. Oxidative and nitrate DNA damage in animals and patients with inflammatory diseases in relation to inflammation-related carcinogenesis. *Biol Chem.* 2006; 387: 365-72.
13. Zhang S, Langer R, Traverso G. Nanoparticulate drug delivery systems targeting inflammation for treatment of inflammatory bowel disease. *Nano Today.* 2017; 16: 82-96.
14. Vong LB, Mo J, Abrahamsson B, Nagasaki Y. Specific accumulation of orally administered redox nanotherapeutics in the inflamed colon reducing inflammation with dose-response efficacy. *J Control Release.* 2015; 210: 19-25.
15. Zhang S, Ermann J, Succi MD, Zhou A, Hamilton MJ, Cao B, et al. An inflammation-targeting hydrogel for local drug delivery in inflammatory bowel disease. *Sci Transl Med.* 2015; 7: 300ra128.
16. Vong LB, Tomita T, Yoshitomi T, Matsui H, Nagasaki Y. An Orally Administered Redox Nanoparticle that Accumulates in the Colonic Mucosa and Reduces Colitis in Mice. *Gastroenterology.* 2012; 143: 1027-36 e3.
17. Zhang QX, Tao H, Lin YY, Hu Y, An HJ, Zhang DL, et al. A superoxide dismutase/catalase mimetic nanomedicine for targeted therapy of inflammatory bowel disease. *Biomaterials.* 2016; 105: 206-21.
18. Cheng Z, Al Zaki A, Hui JZ, Muzykantov VR, Tsourkas A. Multifunctional nanoparticles: cost versus benefit of adding targeting and imaging capabilities. *Science (New York, NY).* 2012; 338: 903-10.
19. Namrata S, Azharuddin SM, Shubhi S, Patrick DS, Govindasamy M. A Redox Modulatory Mn<sub>3</sub>O<sub>4</sub> Nanozyme with Multi-Enzyme Activity Provides Efficient Cytoprotection to Human Cells in a Parkinson's Disease Model. *Angew Chem Int Ed Engl.* 2017; 129: 14455-9.
20. Fan K, Xi J, Fan L, Wang P, Zhu C, Tang Y, et al. In vivo guiding nitrogen-doped carbon nanozyme for tumor catalytic therapy. *Nat Commun.* 2018; 9: 1440.
21. Wei H, Wang E. Nanomaterials with enzyme-like characteristics (nanozymes): next-generation artificial enzymes. *Chem Soc Rev.* 2013; 42: 6060-93.
22. Wu J, Wang X, Wang Q, Lou Z, Li S, Zhu Y, et al. Nanomaterials with enzyme-like characteristics (nanozymes): next-generation artificial enzymes (II). *Chem Soc Rev.* 2019; 48: 1004-76.
23. Zhao J, Cai X, Gao W, Zhang L, Zou D, Zheng Y, et al. Prussian Blue Nanozyme with Multienzyme Activity Reduces Colitis in Mice. *ACS Appl Mater Inter.* 2018; 10: 26108-17.
24. Yao J, Cheng Y, Zhou M, Zhao S, Lin S, Wang X, et al. ROS scavenging Mn<sub>3</sub>O<sub>4</sub> nanozymes for in vivo anti-inflammation. *Chem Sci.* 2018; 9: 2927-33.
25. Youshia J, Lamprecht A. Size-dependent Nanoparticulate Drug Delivery in Inflammatory Bowel Diseases. *Expert Opin Drug Deliv.* 2016; 13: 281-94.
26. Lamprecht A, Schafer U, Lehr CM. Size-dependent bioadhesion of micro- and nanoparticulate carriers to the inflamed colonic mucosa. *Pharm Res.* 2001; 18: 788-93.
27. Jube TT, Nadler-Milbauer M, Barenholz Y, Rubinstein A. Local treatment of experimental colitis in the rat by negatively charged liposomes of catalase, TMN and SOD. *J Drug Target.* 2006; 14: 155-63.
28. Fu G, Liu W, Feng S, Yue X. Prussian blue nanoparticles operate as a new generation of photothermal ablation agents for cancer therapy. *Chem Commun (Camb).* 2012; 48: 11567-9.
29. Zhang W, Hu S, Yin JJ, He W, Lu W, Ma M, et al. Prussian Blue Nanoparticles as Multienzyme Mimetics and Reactive Oxygen Species Scavengers. *J Am Chem Soc.* 2016; 138: 5860-5.
30. Lee Y, Kim H, Kang S, Lee J, Park J, Jon S. Bilirubin Nanoparticles as a Nanomedicine for Anti-inflammation Therapy. *Angew Chem Int Ed Engl.* 2016; 55: 7460-3.
31. Zhang W, Hu S, Yin J-J, He W, Lu W, Ma M, et al. Prussian Blue Nanoparticles as Multienzyme Mimetics and Reactive Oxygen Species Scavengers. *J Am Chem Soc.* 2016; 138: 5860-5.
32. Hua S, Marks E, Schneider JJ, Keely S. Advances in oral nano-delivery systems for colon targeted drug delivery in inflammatory bowel disease: selective targeting to diseased versus healthy tissue. *Nanomedicine.* 2015; 11: 1117-32.